

# Gluon Saturation Effects in Relativistic U+U Collisions

Anthony Kuhlman, Ulrich Heinz,\* and Yuri V. Kovchegov

*Department of Physics, The Ohio State University, Columbus, OH 43210, USA*

(Dated: July 2, 2018)

We examine entropy production in relativistic U+U collisions on the basis of a Color Glass Condensate (CGC) type picture as implemented in the Kharzeev-Levin-Nardi model (KLN). In this framework, we find that the peak entropy density produced in tip-on-tip U+U collisions is about 30% greater than that seen in central Au+Au collisions. Although the resulting difference in the produced charged particle multiplicity between tip-on-tip and side-on-side collisions is smaller than that predicted by previous Glauber model estimates, it is still large enough to allow for experimental discrimination between average orientations of the uranium nuclei. We also point out that in the saturation/CGC approach the collision geometry plays a more important role than previously believed, and that the observed centrality dependence of the produced particle multiplicity per participant in Au+Au collisions can be qualitatively reproduced even without running coupling effects.

PACS numbers: 25.75.-q, 25.75.Nq, 12.38.Mh, 12.38.Qk

Recent studies [1, 2, 3] have pushed for a uranium-uranium (U+U) collision program at RHIC to address a number of unanswered questions about the quark-gluon plasma (QGP). In particular, it is thought [1, 2] that the higher entropy densities produced in U+U over those found in Au+Au collisions would provide a definitive test of the seemingly ideal hydrodynamic behavior of the elliptic flow observed at RHIC [4, 5].

Previous estimates [1, 2, 3] relied on a Glauber model calculation of the entropy densities produced in U+U collisions. These results showed a substantial increase in the initially produced entropy density over that seen in even the most central Au+Au collisions. Perhaps most importantly, a clear ( $\sim 15\%$ ) difference in the multiplicities produced in tip-on-tip versus side-on-side U+U collisions allowed the selection of average relative orientations of the two uranium nuclei, by placing cuts on the charged particle multiplicity [1]. This remains true even if experimental inefficiencies in triggering on full-overlap U+U collisions, using strict spectator nucleon cuts, are taken into account [2].

However, our theoretical understanding of the initial particle production processes during the nuclear collision and the conditions of the produced plasma at early times remains limited, and it has recently been shown [6, 7] that this results in significant ambiguities for the initial source eccentricities in non-central Au+Au collisions at RHIC. Hirano and collaborators [6, 7] found that, if one uses parametrizations for the initial entropy production that are based on the Color Glass Condensate model [8] of gluon saturation in large nuclei at high energies [9], in particular the Kharzeev-Levin-Nardi (KLN) parametrization [10, 11, 12], one obtains initial density profiles in the transverse plane which are flatter and have steeper edges than the more Gaussian-looking profiles [13] one obtains from the Glauber model. As a consequence, one obtains initial source eccentricities which, over most of the impact parameter range, are significantly

larger in the KLN model than in the Glauber model. As shown in Ref. [7], this ambiguity in the initial conditions has considerable impact on the interpretation of available elliptic flow data and the question to what extent the QGP created at RHIC behaves like a “perfect fluid”.

In the present paper we investigate to what extent these model ambiguities for the initial entropy production also affect the usefulness of a U+U collision program where one tries to exploit the intrinsic deformation of the colliding nuclei to generate deformed fireballs even in central collisions. Specifically, we study the influence of various model assumptions about the initial entropy production on the distribution of source eccentricities in U+U collisions, in order to assess how model ambiguities affect our ability to select for specific collision geometries by cutting event samples on the number of spectator nucleons and on charged particle multiplicity [1, 2, 3].

We begin by outlining our procedure for calculating the initial entropy production from the Color Glass Condensate model. We use the KLN parametrization [10, 11], in the specific form implemented by Hirano and Nara in Ref. [12], where the initial energy per unit rapidity and per unit transverse area is given by the  $k_T$ -factorization formula [9]

$$\begin{aligned} \frac{dE}{d^2x_\perp dy} &= \frac{2\pi^3 N_c}{N_c^2 - 1} \int^{p_{\text{cut}}} \frac{d^2p_T}{p_T} \int_0^{p_T} d^2k_T \\ &\times \alpha \left( \max \left\{ \frac{(\mathbf{k}_T - \mathbf{p}_T)^2}{4}, \frac{(\mathbf{k}_T + \mathbf{p}_T)^2}{4} \right\} \right) \\ &\times \phi_A \left( x_1, \frac{(\mathbf{k}_T + \mathbf{p}_T)^2}{4}; \mathbf{x}_\perp \right) \phi_B \left( x_2, \frac{(\mathbf{k}_T - \mathbf{p}_T)^2}{4}; \mathbf{x}_\perp \right), \end{aligned} \quad (1)$$

with  $x_{1,2} = p_T \exp(\pm y)/\sqrt{s}$ . The unintegrated gluon distribution for nucleus  $A$  is taken to be

$$\phi_A(x, k^2; \mathbf{x}_\perp) = \frac{\kappa C_F Q_s^2}{2\pi^3 \alpha_s(Q_s^2)} \begin{cases} \frac{1}{Q_s^2 + \Lambda^2}, & k \leq Q_s, \\ \frac{1}{k^2 + \Lambda^2}, & k > Q_s, \end{cases} \quad (2)$$

where the saturation momentum  $Q_s$  is determined by solving

$$Q_s^2(x, \mathbf{x}_\perp) = \frac{2\pi^2}{C_F} \alpha_s(Q_s^2) xG(x, Q_s^2) n_{\text{part},A}(\mathbf{x}_\perp), \quad (3)$$

and similarly for nucleus  $B$ . The normalization  $\kappa$  in Eq. (2) is fixed by the measured charged particle multiplicity  $dN_{\text{ch}}/dy$  in central Au+Au collisions at  $\sqrt{s} = 200$  A GeV (see below). To reproduce the results of Refs. [7] and [12], we take  $\kappa^2 = 1.8$ .

Both the energy density (1) and the local (i.e.  $\mathbf{x}_\perp$ -dependent) saturation momenta of the two nuclei, Eq. (3), depend on the impact parameter of the collision through the density of wounded nucleons  $n_{\text{part}}$  in the transverse plane, computed from the standard Glauber model formula (see, e.g., Ref. [13]). For nucleus  $A$  it is given by

$$n_{\text{part},A}(\mathbf{r}_\perp, \mathbf{b}) = T_A \left( \mathbf{r}_\perp + \frac{\mathbf{b}}{2} \right) \left( 1 - \left( 1 - \frac{\sigma_{NN} T_B(\mathbf{r}_\perp - \frac{\mathbf{b}}{2})}{B} \right)^B \right), \quad (4)$$

while for nucleus  $B$  the nuclear thickness functions  $T_A$  and  $T_B$  should be interchanged. The latter are computed from a Woods-Saxon distribution for the density of the uranium nucleus, with radius  $R(\theta) = (6.8 \text{ fm})(0.91 + 0.26 \cos^2 \theta)$  (where  $\theta$  is the polar angle with the nuclear symmetry axis) and surface thickness  $\xi = 0.54$  fm.

The integrated gluon distribution,  $xG(x, k^2)$ , in Eq. (3) is given by

$$xG(x, k^2) = K \ln \left( \frac{k^2 + \Lambda^2}{\Lambda_{QCD}^2} \right) x^{-\lambda} (1-x)^4, \quad (5)$$

with  $K = 0.7$  and  $\lambda = 0.2$  [12]. The running coupling constant  $\alpha_s$  is computed from the one-loop expression

$$\alpha_s(k^2) = \frac{4\pi}{\beta_0 \ln \left( \frac{k^2 + \Lambda^2}{\Lambda_{QCD}^2} \right)} \quad (6)$$

with  $\beta_0 = 11 - \frac{2}{3}n_f = 9$ . To render the calculations infrared safe, we limit the growth of the running coupling constant at small  $k^2$  by cutting it off at  $\alpha_s(k^2) = 0.5$  [7]. In all expressions above we use  $\Lambda = \Lambda_{QCD} = 0.2$  GeV [7, 12].

From equation (1) we obtain the energy density at thermalization time  $\tau_0$  (for which we use  $\tau_0 = 0.6$  fm/c) as  $e(\mathbf{x}_\perp, \tau_0) = dE/(\tau_0 d^2x_\perp d\eta)$  at  $\eta = y = 0$ . We then translate this energy density  $e$  into an entropy density  $s$ , by assuming that it thermalizes and using the relationship  $s = 8.67 e^{3/4}$  (where  $e$  must be inserted in GeV/fm<sup>3</sup>) for a thermalized ideal gas of quarks and gluons. By adjusting  $\kappa$ , this entropy density is then normalized such that for impact parameter  $b=0$  its integral over the transverse plane yields the same result as the Glauber model in reference [1] (*cf.* Figure 1).

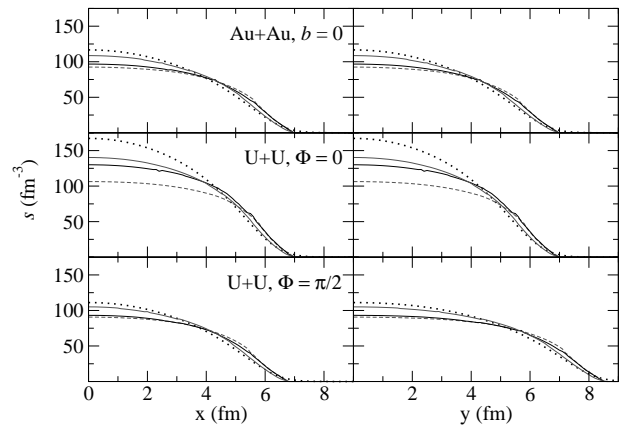


FIG. 1: Transverse entropy density profiles in the in-plane direction (left) compared with those in the out-of-plane direction (right) for central Au+Au (top panels), tip-on-tip U+U (center panels) and side-on-side U+U collisions (bottom panels). Shown are results from the Glauber model (dotted) and from the KLN model with three different  $p_T$  cutoffs (see text):  $p_{\text{cut}} = 3$  GeV/c (dashed gray),  $p_{\text{cut}} = 2 Q_s^{\text{max}}$  (solid black), and  $p_{\text{cut}} = \infty$  (solid gray).

We then assume that the charged particle multiplicity,  $dN_{\text{ch}}/d\eta$ , is proportional to the total entropy produced in the plane,  $dN_{\text{ch}}/d\eta = \Gamma \int d^2r_\perp s(\mathbf{r}_\perp)$ , and adjust the proportionality constant  $\Gamma = 0.088$  to agree with central Au+Au data obtained by the PHOBOS collaboration [14]. The resulting fit is shown in Figure 2. These parameters are then assumed to also describe U+U collisions at the same collision energy.

In the work of Hirano and Nara, the integral over  $p_T$  in Eq. (1) is cut off at a fixed value of  $p_{\text{cut}} = 3$  GeV, to limit the contribution from high- $p_T$  gluons which thermalize incompletely [12]. As shown in Fig. 2, the resulting centrality dependence of the charged particle multiplicity in 200 A GeV Au+Au collisions reproduces the PHOBOS data [14] very well. However, the use of a fixed  $p_T$  cutoff in Eq. (1), independent of impact parameter, raises questions: The momentum dependence of the unintegrated gluon distributions  $\phi_{A,B}$  is controlled by their respective saturation momenta in Eq. (3) which do depend on both  $\mathbf{x}_\perp$  and  $\mathbf{b}$ ; by implementing a fixed cutoff in  $p_T$ , one doesn't allow the  $p_T$  integral to fully explore this  $b$ -dependence. As we discuss now (and show in Figure 2), this leads to a significant distortion of the centrality dependence of charged hadron production.

At any given point  $\mathbf{x}_\perp$  in the overlap region of the two nuclei, the result of equation (1) is controlled by two saturation momenta,  $Q_{s,\text{min}}$  and  $Q_{s,\text{max}}$ , corresponding to the smaller and larger of the nuclear thicknesses of the two colliding nuclei at this point. If we ignore the running of  $\alpha_s$ , the integrand of equation (1) is essentially constant for  $p_T < Q_{s,\text{min}}$ , decreases like  $1/p_T^2$  for  $Q_{s,\text{min}} < p_T < Q_{s,\text{max}}$  and like  $1/p_T^4$  for  $p_T > Q_{s,\text{max}}$ . With a fixed  $p_T$  cutoff we cut off more of the  $1/p_T^4$  tail

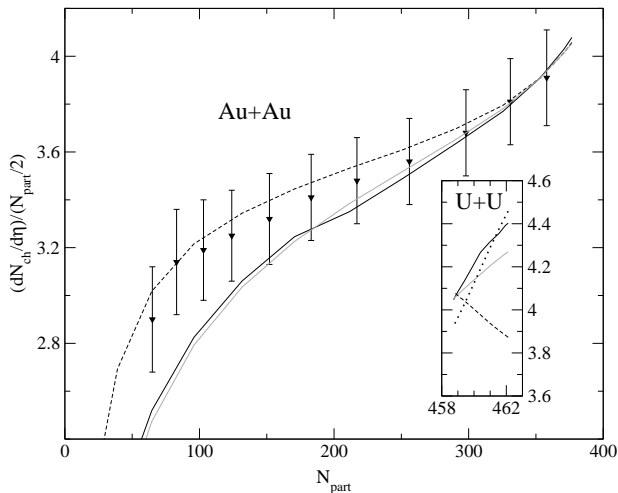


FIG. 2: Charged particle multiplicity per participant pair as a function of centrality for Au+Au. The inset shows corresponding predictions for full-overlap U+U collisions. The data are from PHOBOS at  $\sqrt{s}=200 A_1\text{GeV}$  [14]. Shown are results from the Glauber model (dotted) and from the KLN model different  $p_T$  cutoffs:  $p_{\text{cut}} = 3 \text{ GeV}/c$  (dashed),  $p_{\text{cut}} = 2 Q_s^{\text{max}}$  (black), and  $p_{\text{cut}} = \infty$  (gray).

in central than in more peripheral collisions, due to the fact that  $Q_{s,\text{max}}$  is larger in the former case. The net effect of this is to suppress entropy production in central relative to peripheral collisions. Indeed, the centrality dependence of  $dN_{\text{ch}}/dy$  becomes noticeably steeper if this  $p_T$  cutoff is removed (solid gray line in Figure 2). The same effect can be achieved by allowing the  $p_T$  cutoff to scale with the (centrality dependent) effective saturation momentum. We tested this by setting  $p_{\text{cut}} = 2 Q_s^{\text{max}}(b)$  where we chose (somewhat arbitrarily)  $Q_s^{\text{max}}(b) = Q_s(x=0.01, \mathbf{x}_\perp=\mathbf{0}; \mathbf{b})$  (solid black line in Figure 2).

Even if for Au+Au collisions the effect of removing the  $p_T$  cutoff in Eq. (1) is clearly noticeable in the centrality dependence of  $dN_{\text{ch}}/dy$ , it remains quantitatively small ( $\sim 15\%$  in peripheral collisions). For full-overlap U+U collisions, however, the different ways of cutting off or not cutting off the  $p_T$  integral produce *qualitatively different* results. The inset in Figure 2 shows that for a fixed  $p_T$  cutoff of  $3 \text{ GeV}/c$  (dashed black line), tip-on-tip collisions produce *lower* multiplicities than side-on-side collisions, in stark contradiction with the Glauber model prediction (dotted line). The qualitative tendency of the Glauber model to produce higher multiplicities in tip-on-tip collisions [1, 2, 3] (due to the larger binary collision component in this configuration) is recovered in the KLN saturation model if the  $p_T$  cutoff is either entirely removed (solid gray line) or assumed to scale with the saturation momentum (solid black line). In either case, however, the quantitative difference between tip-on-tip and side-on-side multiplicities is somewhat smaller for the KLN

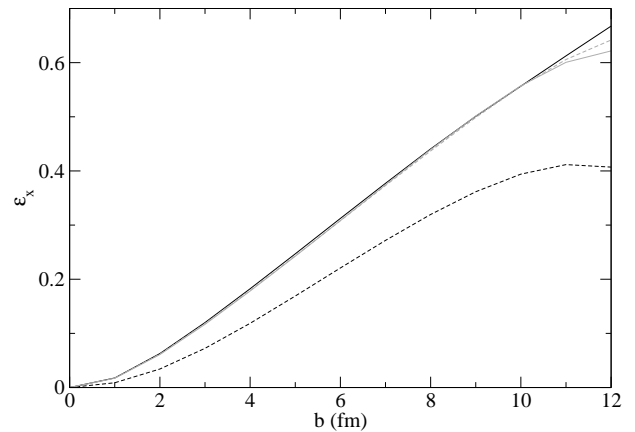


FIG. 3: Eccentricity versus impact parameter for Au+Au collisions at  $\sqrt{s} = 200 \text{ GeV}$  for the Glauber model (dashed) and the KLN model with  $p_{\text{cut}} = 2 Q_s$  (black),  $p_{\text{cut}} = \infty$  (gray) and  $p_{\text{cut}} = 3 \text{ GeV}/c$  (dashed gray).

model than for the Glauber parametrization.

Returning to the initial entropy density profiles shown in Figure 1, we can now see how these differences arise: Generically, the profiles from the saturation model are flatter near the center and steeper near the edge than those from the Glauber model (which look more Gaussian). In tip-on-tip collisions (center panels) the Glauber model shows the strongest growth of entropy density in the middle of the overlap region, due to a strong increase of the binary collision component. This growth is tempered in the KLN saturation model, due to the slower (logarithmic) increase of the saturation momentum  $Q_s$  as one approaches the center of the overlap region. If one implements a fixed  $p_T$  cutoff, the  $p_T$  integral in Eq. (1) can not even fully explore this logarithmic growth of the saturation momentum, and the entropy density increases even more slowly towards the center. In fact, the difference in entropy *density* between tip-on-tip and side-on-side collisions then becomes so small that it can no longer compensate for the smaller overlap area in tip-on-tip collisions, leading to the aforementioned counterintuitive result of *smaller* total multiplicities in tip-on-tip compared to side-on-side collisions (dashed gray line in the inset of Fig. 2).

As already pointed out in Refs. [6, 7], the more plateau-like entropy distributions from the KLN model yield larger eccentricities  $\epsilon_x = \frac{\langle y^2 - x^2 \rangle}{\langle y^2 + x^2 \rangle}$  than the Glauber model profiles, due to their bigger weights at larger distance from the fireball center. In Figure 3 we show the eccentricity of the initial entropy distribution as a function of impact parameter  $b$  for Au+Au collisions. We confirm the observation made in [7] that the KLN eccentricities exceed the Glauber ones by about 25-30% over most of the impact parameter range, and further show that they are insensitive to the choice of the  $p_T$  cutoff in Eq. (1). Since the value of the initial source eccentricity controls

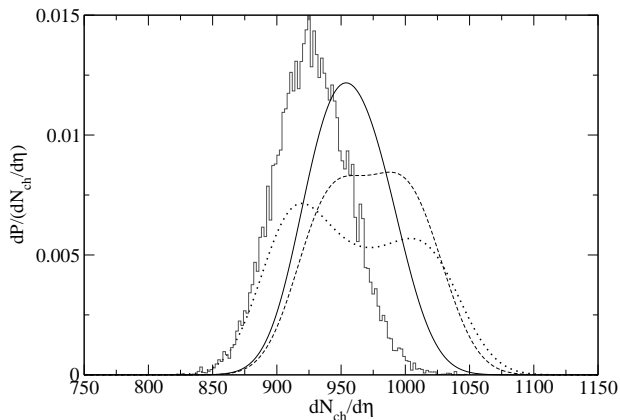


FIG. 4: Multiplicity distribution for full-overlap U+U collisions. Shown are results from the Glauber model (dotted) and the KLN model with  $p_{\text{cut}} = 2Q_s^{\text{max}}$  (dashed) and  $p_{\text{cut}} = \infty$  (solid black). Also shown is the result of cutting the full multiplicity distribution given in Figure 6 on the 0.5% of events with the lowest number of spectators.

the finally observed elliptic flow, Fig. 3 reassures us that the conclusions of Ref. [7] as to the interpretation of the measured  $v_2$  values are not affected by model uncertainties related to the choice of  $p_T$  cutoff.

In [1, 2] two of us advocated using the multiplicity to select for particular orientations of the colliding uranium nuclei. In the Glauber model framework, we found that of all possible orientations of full-overlap U+U collisions, the highest multiplicities were produced in tip-on-tip collisions and the lowest multiplicities were formed in those collisions between nuclei in the side-on-side configuration. The difference in mean multiplicity between these extreme cases was  $\approx 14\%$  [1]. This provided a “handle” to select for average orientations of the nuclei: By selecting events with high multiplicity, one effectively triggers on low source eccentricity, and *vice versa*. The 14% difference in multiplicities between tip-on-tip and side-on-side collisions proved large enough that such a discrimination between collision configurations with large and small source eccentricities remained feasible even after experimental inefficiencies in triggering on full-overlap U+U collisions (by selecting events with a small number of spectator nucleons) were taken into account [2].

The inset in Fig. 2 shows that with CGC/KLN initial conditions the range of multiplicities produced by the different orientations of full-overlap collisions is somewhat smaller than in the Glauber model calculations. It may therefore be prudent to reanalyze the possible degradation of our ability to select event classes of well-defined source eccentricity resulting from trigger inefficiencies and event-by-event multiplicity fluctuations.

We first study the effect of event-by-event multiplicity fluctuations, assuming that full-overlap collisions can be selected with 100% efficiency. As before [1] we adopt as probability distribution for the event-by-event multiplicity

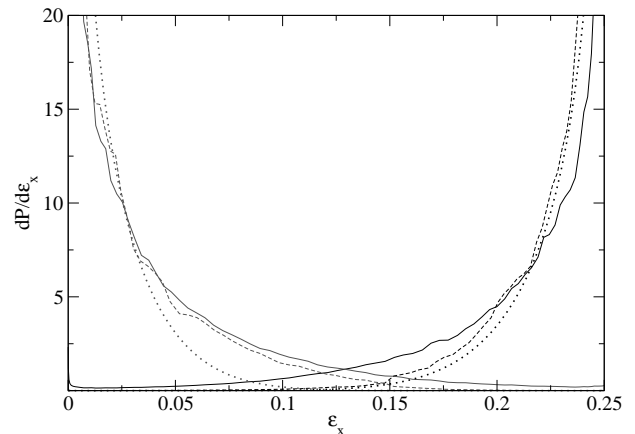


FIG. 5: Eccentricity distributions resulting from cutting the multiplicity distributions of Fig. 4 on the 10% of events with the lowest (black) and highest (gray) multiplicities. Shown are results for the Glauber model (dotted) and the KLN model with  $p_{\text{cut}} = 2Q_s^{\text{max}}$  (dashed) and  $p_{\text{cut}} = \infty$  (solid).

ity the expression [10]

$$\frac{dP}{dn d\Phi} = A \exp \left\{ -\frac{(n - \bar{n}(\Phi))^2}{2a\bar{n}(\Phi)} \right\}, \quad (7)$$

where  $n$  is the measured multiplicity in a given event and  $\bar{n}(\Phi)$  is the average multiplicity for a given orientation  $\Phi$  of the nuclei, now computed from the KLN model using the procedure described above. For the parameter  $a$  controlling the width of the fluctuations we again take  $a = 0.6$  as this has been shown to produce good agreement with existing Au+Au data [10].

Integrating Eq. (7) over  $\Phi$  yields the multiplicity distribution for full-overlap U+U collisions, shown in Fig. 4. As expected, the distributions obtained from the KLN model are considerably narrower than the one resulting from the Glauber model. Furthermore, the shapes of the distributions are quite different, a result of the individual Gaussian distributions from tip-on-tip and side-on-side collisions being squeezed on top of one another, due to the smaller difference in mean multiplicity between them.

After placing cuts on the multiplicity distributions of Fig. 4, we can convert the multiplicity distribution into a distribution of eccentricities according to

$$\frac{dP}{d\epsilon_x} \Big|_{n_0}^{n_1} = \int_{n_0}^{n_1} dn \frac{dP}{dn} \frac{d\Phi}{d\epsilon_x}, \quad (8)$$

where  $n_0$  and  $n_1$  represent the lower and upper limits of the multiplicity cuts, respectively. The resulting eccentricity distributions are shown in Fig. 5 for cuts on events with the 10% lowest and highest multiplicities, respectively. Not unexpectedly, the distributions resulting from the KLN model are slightly broader than those from the Glauber model: Due to the smaller range of multiplicities between the  $\Phi = 0$  and  $\Phi = \frac{\pi}{2}$  configurations, the

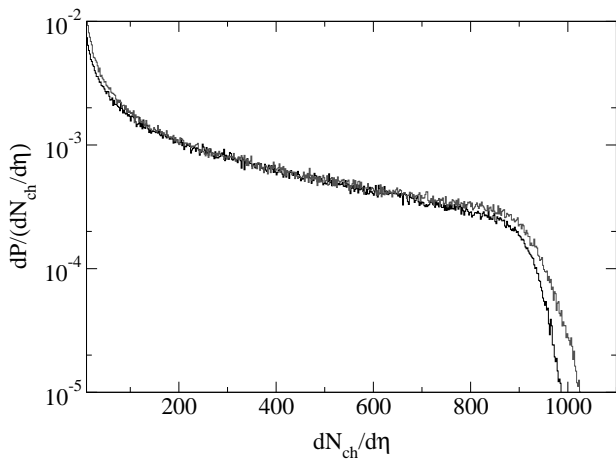


FIG. 6: Multiplicity distribution for U+U collisions with arbitrary impact parameters and relative orientations. The gray curve corresponds to the Glauber model calculation of Ref. [2] while the result from the KLN model is given by the solid curve.

eccentricities corresponding to given multiplicity slice are less sharply defined. This also results in a slightly higher (lower) average eccentricity of high (low) multiplicity samples: For the high multiplicity cut, the KLN model (with the  $p_T$  cutoff choices listed in Fig. 5) gives an average eccentricity  $\langle \epsilon_x \rangle = 0.03-0.04$  (vs.  $\langle \epsilon_x \rangle = 0.014$  from the Glauber model), whereas for the low multiplicity cut the KLN model gives  $\langle \epsilon_x \rangle = 0.22-0.23$  (vs.  $\langle \epsilon_x \rangle = 0.24$  from the Glauber model). We conclude that the differences between the two classes of models are small, and the suggested event selection scheme remains feasible in this new framework. [It is worth noting that we have computed these same eccentricity distributions for energies that will be available at the LHC and found no significant deviations from the results presented here.]

We now proceed to also discuss the effects of trigger inefficiencies in the selection of full-overlap collisions on the eccentricity selection. We repeat the calculations reported in Ref. [2] for the KLN model, restricting our attention to the case without  $p_T$  cutoff ( $p_{\text{cut}} \rightarrow \infty$ ). Figure 6 gives the resulting complete multiplicity distribution for U+U collisions of any impact parameter and relative orientation, and compares it with the previously studied Glauber model initialization. The most notable feature is the reduced width of the high-multiplicity tail in the KLN model, due to the smaller spread of multiplicities in  $b=0$ , full-overlap collision events seen in Fig. 4. The latter can be selected from this distribution by placing very strict cuts on the number of spectator nucleons. The gray histogram in Fig. 4 shows the multiplicity distribution for an event class that was obtained by selecting from the KLN distribution in Fig. 6 the 0.5% events with the lowest spectator counts. If we cut this multiplicity distribution once more for high (low) multiplicities, we

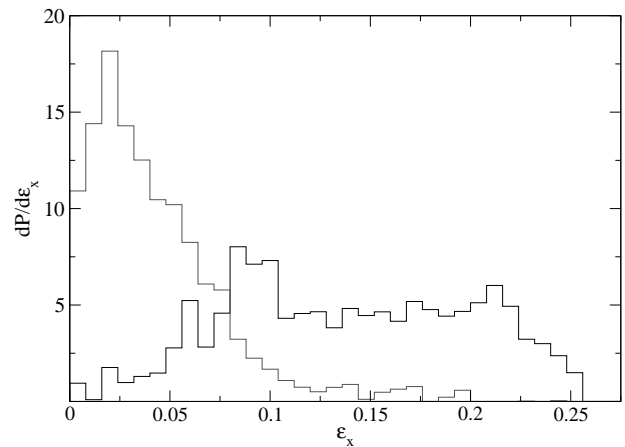


FIG. 7: Eccentricity distributions resulting from cutting the gray histogram in Figure 4 on the 5% of events with the lowest (black) and highest (gray) multiplicities. The corresponding average eccentricities are 14% (black) and 4% (gray).

can again select events with small (large) average eccentricity.

The resulting eccentricity distributions are shown in Fig. 7. The black (gray) histogram corresponds to the subclass of events obtained by selecting from the gray histogram in Fig. 4 the 5% lowest (highest) multiplicity events. While the eccentricities are rather widely distributed within these two event subclasses, their average eccentricities are very different:  $\langle \epsilon_x \rangle = 0.04$  for the high-multiplicity subclass vs.  $\langle \epsilon_x \rangle = 0.14$  for the low-multiplicity selection. (For the Glauber model the corresponding average eccentricities were 0.02 and 0.18, respectively, and actual values distributed somewhat more narrowly about these averages [2].)

We conclude that, in spite of the documented quantitative differences between the initial entropy distributions calculated from the KLN and Glauber models, the proposed event selection scheme for U+U collisions continues to allow isolating event classes with widely different source eccentricities, at energy and entropy densities that exceed those reachable in Au+Au collisions by a wide margin. Detailed comparisons of elliptic flow measurements in U+U collisions with ideal fluid dynamical calculations will, however, be affected by these model uncertainties.

Before closing, we would like to point out the important role played by the collision geometry in determining from the saturation model the centrality dependence of particle multiplicity per participant. For simplicity, let us assume that the multiplicity of produced gluons at a given location  $\mathbf{x}_\perp$  in transverse plane is given by

$$\frac{dN}{d^2x_\perp dy} \propto \min\{Q_{s1}^2(\mathbf{x}_\perp), Q_{s2}^2(\mathbf{x}_\perp)\}. \quad (9)$$

Here  $Q_{s1}^2(\mathbf{x}_\perp)$  and  $Q_{s2}^2(\mathbf{x}_\perp)$  are the saturation scales in the two colliding nuclei at the given transverse position

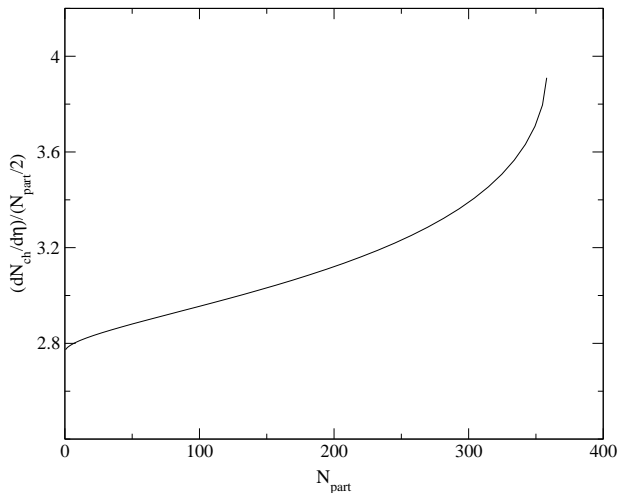


FIG. 8: Particle multiplicity per participant as a function of centrality, for the simple CGC-motivated geometrical model Eq. (9). The proportionality constant in Eq. (9) is chosen to fit the most central data point from [14] (see text for details).

$\mathbf{x}_\perp$ . Equation 9 captures with logarithmic accuracy the main qualitative behavior of integrated particle multiplicity in the saturation/CGC approach. It can be obtained from Eq. (1) if one neglects logarithms of saturation scales as slowly-varying corrections to the power-law scaling of Eq. (9).

For illustration, let us consider a collision of two spherical nuclei (e.g. a Au+Au collision). If the radius of the nuclei is  $R$  and they collide at impact parameter  $\mathbf{b}$ , the saturation scales are (assuming box-like nuclear density distributions for simplicity)

$$\begin{aligned} Q_{s1}^2(\mathbf{x}_\perp) &\propto \sqrt{R^2 - (\mathbf{x}_\perp + \frac{1}{2}\mathbf{b})^2}, \\ Q_{s2}^2(\mathbf{x}_\perp) &\propto \sqrt{R^2 - (\mathbf{x}_\perp - \frac{1}{2}\mathbf{b})^2}, \end{aligned} \quad (10)$$

with the same proportionality coefficient for both of them. Remembering that the square of the saturation scale is proportional to the density of participants  $n_{\text{part}}(\mathbf{x}_\perp)$ , we deduce that the initial gluon (and thus also the final charged hadron) multiplicity per participant is proportional to

$$\frac{1}{N_{\text{part}}} \frac{dN_{\text{ch}}}{dy} \propto \frac{\int d^2x_\perp \min\{Q_{s1}^2(\mathbf{x}_\perp), Q_{s2}^2(\mathbf{x}_\perp)\}}{\int d^2x_\perp (Q_{s1}^2(\mathbf{x}_\perp) + Q_{s2}^2(\mathbf{x}_\perp))}, \quad (11)$$

with the total number of participant nucleons

$$N_{\text{part}} \propto \int d^2x_\perp (Q_{s1}^2(\mathbf{x}_\perp) + Q_{s2}^2(\mathbf{x}_\perp)). \quad (12)$$

The integrals in Eqs. (11) and (12) with the saturation scales (10) can be done numerically, yielding the plot of particle multiplicity per participant as a function of  $N_{\text{part}}$  shown in Fig. 8. The normalization of both axes

was adjusted to fit the most central data point in Fig. 2. The curve in Fig. 8 is seen to qualitatively reproduce the monotonous rise of  $(1/N_{\text{part}})dN_{\text{ch}}/dy$  with  $N_{\text{part}}$  observed at RHIC [14] (see Fig. 2). We stress that the positive slope of the curve in Fig. 8 arises entirely from the geometry of the colliding nuclei, as implemented in the simple CGC-inspired model Eq. (9) for particle production. It is likely that a similar geometrical mechanism is responsible for the positive slope of the gluon multiplicity per participant obtained in numerical simulations of classical gluon fields performed in [15]. Although often stated otherwise, running coupling and/or other logarithmic effects appear *not* to be necessary to obtain this positive slope, but they seem to be required to turn the qualitative agreement of Fig. 8 with the data in Fig. 2 into a quantitative one. Still, we are amazed how well the data shown in Fig. 2 can be qualitatively understood within the simple geometrical saturation model of gluon production given in Eq. (9).

Although a number of different questions can be studied with U+U collisions [1, 16, 17, 18], perhaps the most persuasive argument in favor of a U+U program at RHIC is the potential [1] to test the ideal hydrodynamic behavior of the elliptic flow at higher entropy densities and with larger fireballs than are available in even the most central Au+Au collisions. In the Glauber model calculations presented in [1, 2] we found that the maximum entropy density available in tip-on-tip U+U collisions was approximately 40% greater than that seen in central Au+Au. Examination of Figure 1 leads to a similar conclusion for the KLN model results, with increases of 35% and 29% for the cases with variable and infinite  $p_T$  cutoff, respectively. Since the initial maximum entropy density scales roughly (although not exactly [3]) with the observable  $(1/\langle S \rangle)(dN_{\text{ch}}/dy)$ , where  $\langle S \rangle$  is the mean transverse overlap area of the two colliding nuclei, this increase in initial entropy density provides an important lever arm for testing the approach towards ideal fluid dynamical behavior at RHIC experimentally. The additional parameter space opened up by U+U collisions at RHIC could prove even more important if Pb+Pb collisions at the Large Hadron Collider LHC (which are expected to produce *much* higher initial entropy densities and temperatures) turned out to produce a more weakly coupled quark-gluon plasma than RHIC collisions, and the QGP created at RHIC thus were to yield the best possible approximation of a “perfect fluid”. In this case the U+U collision program could cover a key window in parameter space, but we also note that fully exploiting it would depend on our ability to gain sufficient control over the presently remaining model uncertainties for initial particle production, as studied here.

We wish to thank T. Hirano and D. Kharzeev for particularly illuminating discussions. This work was supported by the U.S. Department of Energy under contract DE-FG02-01ER41190 (UH and AK) and OJI Grant No. DE-FG02-05ER41377 (YuK).

---

\* Correspond to heinz@mps.ohio-state.edu

- [1] U. Heinz and A. Kuhlman, Phys. Rev. Lett. **94**, 132301 (2005).
- [2] A. J. Kuhlman and U. Heinz, Phys. Rev. C **72**, 037901 (2005).
- [3] C. Nepali, G. Fai and D. Keane, Phys. Rev. C **73**, 034911 (2006).
- [4] BRAHMS Collaboration, I. Arsene *et al.*, Nucl. Phys. A **757**, 1 (2005); PHOBOS Collaboration, B. B. Back *et al.*, *ibid.* **757**, 28 (2005); STAR Collaboration, J. Adams *et al.*, *ibid.* **757**, 102 (2005); PHENIX Collaboration, K. Adcox *et al.*, *ibid.* **757**, 184 (2005).
- [5] P. F. Kolb and U. Heinz, in *Quark-Gluon Plasma 3*, edited by R. C. Hwa and X.-N. Wang (World Scientific, Singapore, 2004), p. 634.
- [6] A. Adil, M. Gyulassy and T. Hirano, arXiv:nucl-th/0509064.
- [7] T. Hirano, U. Heinz, D. Kharzeev, R. Lacey and Y. Nara, Phys. Lett. B, in press [arXiv:nucl-th/0511046].
- [8] E. Iancu, A. Leonidov and L. McLerran, in *QCD Perspectives on Hot and Dense Matter*, edited by J.-P. Blaizot and E. Iancu, NATO Science Series II: Mathematics, Physics, and Chemistry, Vol. 87, p. 73 (Kluwer, Dordrecht, The Netherlands, 2002) [arXiv:hep-ph/0202270]; J. Jalilian-Marian and Y. V. Kovchegov, Prog. Part. Nucl. Phys. **56**, 104 (2006) [arXiv:hep-ph/0505052].
- [9] L. V. Gribov, E. M. Levin and M. G. Ryskin, Phys. Rept. **100**, 1 (1983).
- [10] D. Kharzeev and M. Nardi, Phys. Lett. B **507**, 121 (2001).
- [11] D. Kharzeev and E. Levin, Phys. Lett. B **523**, 79 (2001); D. Kharzeev, E. Levin and M. Nardi, Phys. Rev. C **71**, 054903 (2005); D. Kharzeev, E. Levin and M. Nardi, Nucl. Phys. A **730**, 448 (2004).
- [12] T. Hirano and Y. Nara, Nucl. Phys. A **743**, 305 (2004).
- [13] P. F. Kolb, U. Heinz, P. Huovinen, K. J. Eskola and K. Tuominen, Nucl. Phys. A **696**, 197 (2001).
- [14] B. B. Back *et al.* [PHOBOS Collaboration], Phys. Rev. C **65**, 061901 (2002).
- [15] A. Krasnitz, Y. Nara and R. Venugopalan, Nucl. Phys. A **717**, 268 (2003) [arXiv:hep-ph/0209269].
- [16] Bao-An Li, Phys. Rev. C **61**, 021903(R) (2000).
- [17] E. V. Shuryak, Phys. Rev. C **61**, 034905 (2000).
- [18] P. F. Kolb, J. Sollfrank, and U. Heinz, Phys. Rev. C **62**, 054909 (2000).